Change Detection Using Time and Look Angle Series of Geocoded TanDEM-X Staring Spotlight Images

Knut Eldhuset

***Abstract*—This work describes the analysis of changes in time and look angle series of TanDEM-X (TDX) and TerraSAR-X (TSX) staring spotlight images over the regions around Kjeller near Oslo in Norway and the town Nikel in Russia near the Norwegian border. It is shown that change detection may be done with TDX/TSX with shorter intervals than the repeat cycle using time series of geocoded images with varying look angles. Using look angle series of geocoded images can help to identify changes due to look angle variation. Accurate science orbit data and very good overlap of scenes both in time and look angle make the TDX/TSX data very attractive for both coherent and incoherent change detection.**

***Index Terms*—Synthetic aperture radar (SAR), interferometry, coherence, DEM, geocoding, changes, time series, look angle series.**

I. INTRODUCTION

THE primary objective of the TanDEM-X mission was to generate a global digital elevation model (DEM) [1], a High Resolution DEM (HDEM) with 12 m horizontal resolution. In addition, the system was reconfigurable with several other modes such as the staring spotlight mode with resolution better than 1m. In [2] we focused on generation and estimation of the height accuracy of geocoded DEMs with 1.8 m resolution generated from staring spotlight data from the pursuit mono-static mode. Different aspects around the SAR optimization and performance analysis of staring spotlight mode of TerraSAR-X satellite (which is similar to TanDEM-X) can be found in [3]. The papers in [3] and several references therein explain how the azimuth resolution is substantially improved using staring spotlight compared to sliding spotlight. A new product which is called TanDEM-X Change DEM will be available in 2020 and will substitute the HDEMs. The Change DEM will show the changes in the Earth topography from 2010-2014 to 2017-2019 ([4]). In this paper we will use geocoded TanDEM-X staring spotlight data from the science phase (October 2014-March 2015) to analyse variation of the coherence and amplitudes in time due to changes of the properties of the imaged surface. We use the DEMs generated in [2] to geocode time series of images with either constant look angle or varying look angle using the accurate orbit data. By using images with different look angles we can use time series with shorter time intervals between the scenes than the repeat cycle which is 11 days for TDX/TSX.

Much of the work in the literature on SAR coherent change detection has been focused on analysis of data from stacks of repeated-pass SAR images [5]. Many of these studies are dependent on persistent scatterers [6] in order to detect changes caused by human activities or natural disasters since most reflecting targets decorrelate after some days. Using interferometric pairs from TDX/TSX with a very small time separation provides unique opportunity to generate coherence images and DEMs with unprecedented high coherence. In this work we analyse time series of such coherence images to detect changes. We use such high coherent DEMs to geocode amplitude images for study of incoherent changes in foreign regions where existing digital terrain models (DTM) may be quite coarse.

If we want to detect temporal changes of buildings and infrastructure in time series with look angle variations, we will show that it is necessary to first find out how look angle variation change the backscatter. Look angle variations in themselves may tell something about the structure of buildings and other objects. We show time series with varying look angles of fields and cropland which may be challenging without having good models for backscattering. We show examples of parking areas with cars or buses as well as trains and railway tracks. Activities on ice-covered lakes or rivers and snow-covered roads are also demonstrated. Temperature recordings and snow depths have been collected to help to understand backscatter changes from the ground. The results in this paper which are not dependent on cold climate with ice and snow can be extended to other warmer areas of the globe.

II. TDX MODES AND DATA SETS

A. TDX modes

We received TDX/TSX Co-registered Single-look Slant range Complex (CoSSC) data in HH polarization during the science phase from German Aerospace Center (DLR) under an Announcement of Opportunity project (AO-

This work was supported by the Norwegian Defence Research Establishment (FFI). (*Corresponding author: Knut Eldhuset.*)

Knut Eldhuset is with the Norwegian Defence Research Establishment, Department of Sensor and Surveillance Systems, Kjeller Norway (e-mail: Knut.Eldhuset@ ffi.no).

projectNTI_INS6664). The science phase started in October 2014 and was completed in December 2015. Within this time, two main interferometric operation modes were executed: the pursuit monostatic mode (October 2014–February 2015) and the bi-static mode (March 2015–December 2015). In the pursuit mono-static mode, the two satellites operated independently with an along-track distance of 76 km (10 s temporal separation). In the bi-static mode, the along-track distance was mostly less than 500 m and either TSX or TDX was used as a transmitter and both satellites received the scattered echo. In this paper we only study the images from the pursuit monostatic mode. For further details on the modes and science phase timeline, please refer to [7]. The processing of CoSSC products has been described in [8].

B. *Data set*

We received data sets from both the mono-static and bi-static modes for generation of DEMs [2] . Three test sites were selected in the AO-project. For the analysis in this paper we use two of them, Kjeller and Nikel. Nikel is a foreign area in Russia close to the Norwegian border and Kjeller is a well- known area close to Oslo. The scenes over Kjeller are listed in Table I and those from Nikel are listed in Table II. In Table I there are two scenes with only one day separation, which may be useful for short time change detection.

In the data set we received from Nikel ([2]) there were 3 scenes which are listed in Table II with one day interval at incidence angles 51.9°, 41.5° and 27.6° and on 7, 8 and 9 January, respectively. In this paper we also study three other scenes at incidence angle 41.5° on 8 January, 19 January and 10 February. In Table II there are 6 scenes at incidence angle 35.0° which we use to illustrate some interesting changes in coherence.

TABLE I
ASCENDING RIGHT-LOOKING TSX/TDX COSSC INTERFEROMETRIC PAIRS FROM TEST SITE KJELLER

	Date	Amb (m)	Inc(°)	Coherence
ST mono-static	22 December 2014	-26.6	49.622	0.59
ST mono-static	9 March 2015	16.8	49.612	0.57
ST mono-static	10 March 2015	14.8	32.415	0.67
Strip map bi-static	1 November 2015	-62.1	42.672	0.73

The scene centre is (59 º 59′ 10″ N, 11º 3′ 0″ E) and the size of staring spotlight (ST) scenes is around 3 km × 6 km. The pixel size in azimuth is 0.17 m and in range 0.79 m. The height of ambiguity (Amb), Incidence angle (Inc) and mean coherence over a scene are listed in the table.

TABLE II
ASCENDING RIGHT-LOOKING TSX/TDX COSSC INTERFEROMETRIC PAIRS FROM TEST SITE NIKEL

	Date	Amb (m)	Inc(°)	Coherence
ST mono-static	23 December 2014	-17.6	34.968	0.83
ST mono-static	3 January 2015	-11.8	34.987	0.77
ST mono-static	14 January 2015	-13.3	34.986	0.78
ST mono-static	16 February 2015	11.7	34.980	0.76
ST mono-static	27 February 2015	-11.1	34.989	0.71
ST mono-static	10 March 2015	17.5	34.989	0.81
ST mono-static	8 January 2015	-11.4	41.452	0.72
ST mono-static	19 January 2015	-20.0	41.453	0.78
ST mono-static	10 February 2015	17.1	41.454	0.75
ST mono-static	7 January 2015	-13.4	51.866	0.62
ST mono-static	9 January 2015	-10.0	27.600	0.79
Strip Map bi-static	21 October 2015	-65.0	40.703	0.81

The scene centre is (69 º 24′ 36″ N, 30º 12′ 11″ E) and the size of staring spotlight (ST) scenes is around 3 km × 6 km. The pixel size in azimuth is 0.17 m and in range 0.79 m.

III. PROCESSING FROM COSSC DATA TO GEOCODED RGB COLOUR COMPOSITE

All processing algorithms from the CoSSC interferometric pairs have been developed at FFI during many years. The Stereo Interferometric SAR (StInSAR) algorithm combines stereoSAR and InSAR for generation of geocoded DEM, amplitude images and coherence images ([2, 10, 11 (§6, §7, §8)]). In this algorithm the SAR pixel position algorithm described in [9] is used to geolocate pixels. It was shown that the absolute height and geographic position of corner reflectors could be estimated with accuracy of a few decimeters when the science orbit data in the TSX/TDX products was used. This accuracy is therefore sufficient to co-registrate geocoded images with pixel spacing 1-2 m.

DTMs with 10 m pixel spacing from the Norwegian Mapping Authority (NMA) (www.kartverket.no) were used as an aid in phase unwrapping of interferograms over Kjeller. For the Russian test site Nikel, we used DTMs found in Viewfinder Panoramas. At both test sites we used TDX/TSX stripmap CoSSC data in Tables I and II for generation of intermediate DEMs since the height of ambiguity of the strip map interferograms are around 60 m, which is 2-6 times larger than for the staring spotlight interferograms (see more details in [2, 11 (§6, §7, §8)]).

The amplitude and coherence images and the DEMs were all geocoded to WGS84 UTM (Universal Transverse Mercator) projection. The UTM images have a fixed pixel spacing in Northing and Easting coordinates with a common south west corner, hence, the RGB (Red, Green, Blue) images can simply be generated by finding the same easting and northing coordinate in the R, G and B image. The simplest way and the most used method to co-register slant range SAR images with almost equal incidence angles is to cross correlate the images [12]. This method doesn't need any accurate orbit data, however, images with large regions with low contrast may be a problem. Furthermore, it may be difficult or impossible to cross correlate when the incidence angles (and slant range pixel spacings) are different.

IV. ANALYSIS OF CHANGES IN COHERENT AND INCOHERENT IMAGES

A. Images from the Kjeller test site

In [11 (§6, §7, §8)] (in Norwegian, Google translator may be used) we did an analysis of changes with three images at incidence angle 49°. Both amplitude and coherence changes were analysed for the Kjeller airport, the rivers Nitelva and Leira, cropland, forest, urban area, railway track and roads. Especially over cropland there are large variations dependent on snow cover, ice and kind of cultivated land.

Fig. 1 shows a geocoded RGB colour composite generated from three images on 22 December 2014, 9 March 2015 and 10 March 2015 in Table I. The R and G images have incidence angle 49.6° and the B image has incidence angle 32.4°. The B image is skewed compared to the R and G images because the same area is observed from different directions from space. The blue colour is dominant in flat regions since the incidence angle is considerably smaller than for the two other images. However, there is variation in the blue colour from different kind of cropland which may be caused by different temperature. The temperature is some degrees below the freezing point on 22 December and some degrees above the freezing point on 9 and 10 March. Hence, the backscatter may be somewhat stronger with a weak red colour in some fields on 22 December even if incidence angle is larger than on 10 March. It is easily seen that the railway track and much of the urban structures are mainly grey level, which means that the backscatter is quite stable as a function of both time and incidence angle.

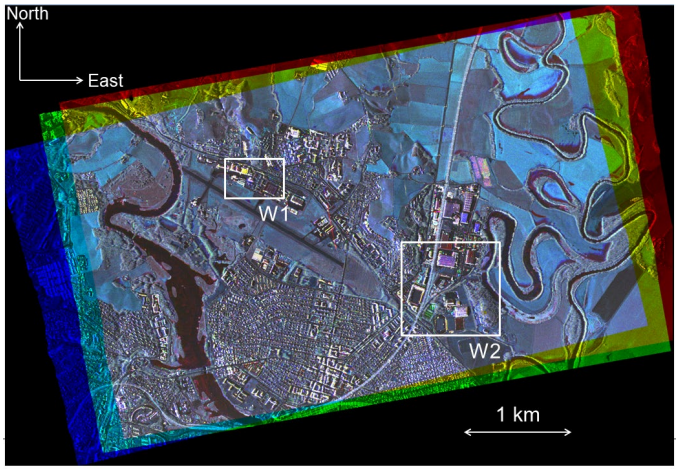

Fig. 1. UTM geocoded RGB colour composite from 22 December 2014 (R), 9 March 2015 (G) and 10 March 2015 (B) where the incidence angles are 49.6°, 49.6° and 32.4° , respectively.

We shall look in more detail into the two windows in Fig. 1, W1 and W2. Fig. 2(a) shows the StInSAR DEM from TDX/TSX in window W2 and Fig. 2(b) shows a DEM generated by NMA by laser scanning with an aircraft in the same area. The DEMs shown here are actually Digital Surface Models (DSM). In [2] we estimated the height of some of the buildings in Fig. 2. The StInSAR heights of buildings B1, B2 and B3 in Fig. 2(a) were 9.6 m, 14.6 m, and 23.2 m, respectively. The heights measured from the laser scanning DEM on the same buildings in Fig. 2(b) are 10.2 m, 15.6 m and 23.8 m, respectively. The differences are 0.6 m, 1.0 m and 0.6 m, which means that the StInSAR heights are somewhat lower compared to the laser DEM. The reason for the difference may be different scattering mechanisms from different types of roofs for radar and laser. It should also be mentioned that the pixel spacing is about 0.5 m for the laser DEM (at least two points per square meter) and 1.8 m for the SAR DEM.

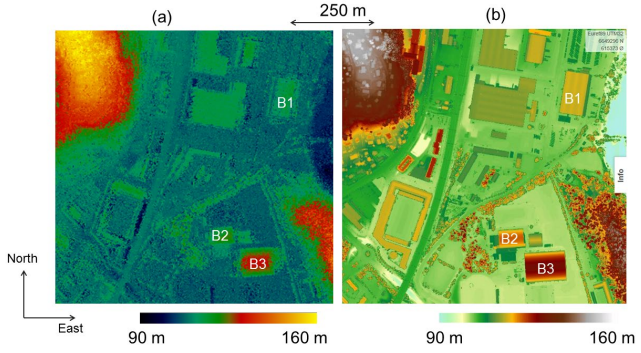

Fig. 2. (a) UTM SAR DEM generated from TanDEM-X in 2015. The pixel spacing is 1.8 m. (b) UTM DEM from aircraft laser scanning in 2017. The pixel spacing is 0.5 m.

Fig. 3(b) is an enlarged image within window W2 in Fig. 1. Fig. 3(a) shows a shadow relief on the laser scanning surface model in Fig. 2(b). R is a railway track, P1 is a parking area for cars, P2 is a parking area for buses, B2 and B3 are sport halls. In Fig. 3(b) we can see that there are cars only in the G image. This is a parking area for the sports halls B2 and B3. The R and

G image are taken on Monday and the B image on Tuesday, all at 6.03 p.m. local time. Monday and Wednesday are a typical day for activities in these sports halls. Monday 22 December is close to Christmas, hence, the cars are absent. On the parking area P2 with buses there is both R, G and B and a mix of them. The sports hall B3 has mostly white stripes across the roof. These are steel arches carrying a light sandwich structure roof. There are actually 10 arches. The 8 arches in the middle are grey or white which means that the scattering in the R, G and B image is roughly the same. In the slant range image the arches look curved (see [2, 11 (§6, §7, §8)]), however, in the geocoded image, nine of the archs have been straightened. This means that the StInSAR DEM is quite accurate. The

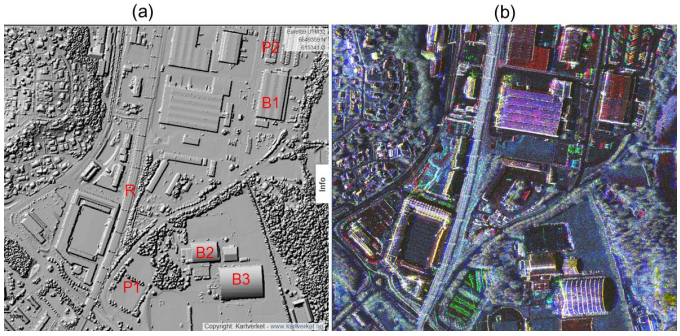

Fig. 3. (a) Shadow relief at 40° solar elevation on the surface model from laser scanning. (b) RGB colour composite in window W2 in Fig. 1.

arches are co-registered very well in all three geocoded images. The arch at the end of the building on the right side is yellow, which means that the scattering in the B image (incidence 32°) is lower than in the R and G images. We can see that building B1 and the neighbour building are mostly red. There were no snow on all dates. The average temperature on 22 December was -6.5°C, on 9 March it was 6.6°C and 6.5°C on 10 March. Some ice on the roof on 22 December and wet or dry roofs on the other dates may be possible. The backscattering may therefore be larger on 22 December.

Fig. 4(b) shows an enlarged image in the window W1 in Fig. 1 which shows some buildings at Kjeller airport. Fig. 4(a) shows a shadow relief on a laser scanning surface model. On building B4 the scattering in image B (incidence 32°) seems to be absent and the scattering in the R and G images is almost the same (R+G=yellow). The ventilation hatches are visible both in the laser scanning image (Fig. 4(a)) and in the SAR RGB colour composite (Fig. 4(b)). This means again that the R, G and B images are very well co-registered. There are few cars (both R, G and B) on parking area P4. On parking area P5 near a school there are cars only in the B image on 10 March in the afternoon at 6 p.m. The scattering from the field in the lower left corner seems to be dominated by the B image at 32.4°.

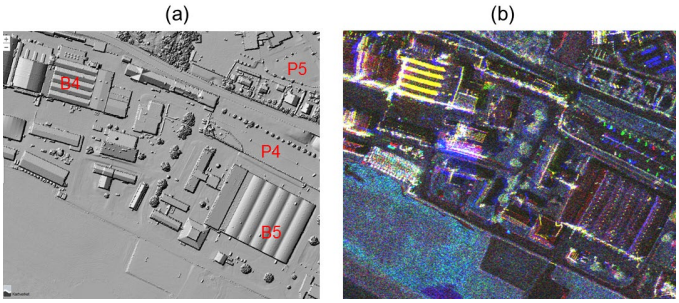

Fig. 4. (a) Shadow relief at 40° solar elevation on the surface model from laser scanning in 2017. The pixel spacing is 1.8 m for the SAR DEM and 0.5 m for the laser DEM . (b) RGB colour composite in window W1 in Fig. 1.

B. Images from the Nikel test site

Fig. 5 shows a UTM geocoded RGB colour composite generated from three images on 8 January, 19 January and 10 February 2015 in Table II, all at incidence angle 41°. The area is around Nikel in Russia close to the Norwegian border which follows one of the hydropower lakes in the Pasvik river. Parts of the ice-covered lake can be seen to the left in the image. The nickel smelter is placed within window W3. The RGB colour composite

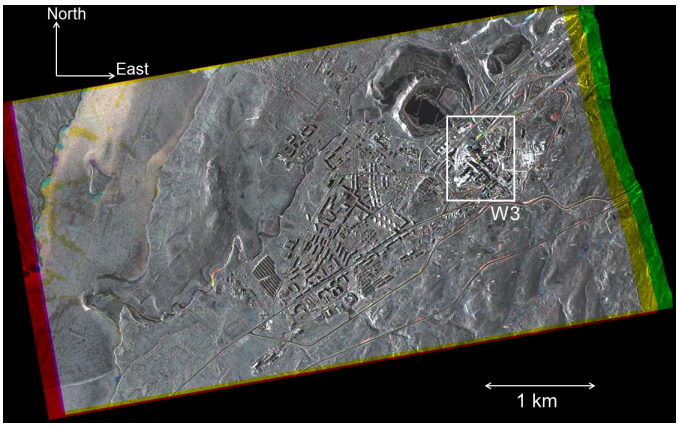

Fig. 5. RGB UTM geocoded image over Nikel on 8 January 2015 (R), 19 January 2015 (G) and 10 February 2015 (B), where the incidence angle is 41° in all images. The pixel spacing is 1.8 m.

is mostly grey level, which means that most of the ground reflections are very stable between the acquisition dates. This is due to the cold climate mostly below zero in both January and February. We have recordings of temperature from a Norwegian meteorological station at Svanvik around 10 km from Nikel. The average temperatures were -5.8°, -9.6° and -3.1° on the dates of the images in Fig. 5. Areas with some activity or natural changes are coloured.

Fig. 6 shows a UTM geocoded RGB colour composite generated from three images on 7 January, 8 January and 9 January in Table II. This RGB colour composite yields the possibility to see changes with 1 day interval. However, the incidence angles are quite different which causes changes in backscattering. If we compare Fig. 5 and Fig. 6 we can find out where changes in backscattering is caused by changes in look angle if the reflecting objects are stable. If the reflections are

RGB grey level in Fig. 5 and RGB colour in Fig. 6, the changes in Fig. 6 must be due to look angle changes. We can see that Fig. 6 is dominated by blue colour all over the image, which is due to a smaller incidence angle and higher backscatter for image B than for images R and G. In both Fig. 5 and Fig. 6 there are local changes on the Pasvik hydro power lake which is caused by water coming up in the cracks in the ice. Fig. 5 and Fig. 6 show that the overlap of the R, G and B images is extremely good, which is important for small scenes in staring spotlight mode.

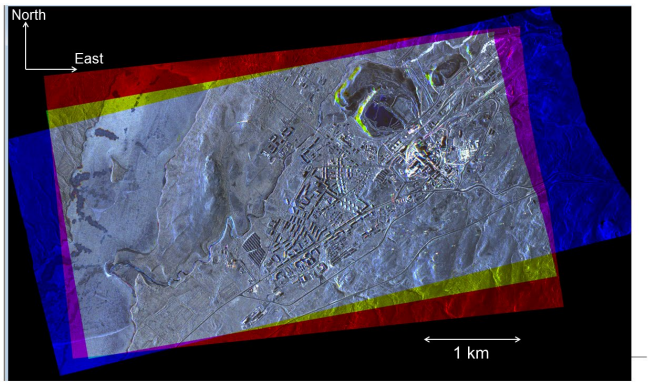

Fig. 6. RGB UTM geocoded image over Nikel on 7 January 2015 (R), 8 January 2015 (G) and 9 January 2015 (B), where the incidence angles are 52°, 41°, 27° , respectively. Pixel spacing is 1.8 m.

Fig. 7(a) shows the area within the window W3 in Fig. 5, while Fig. 7(b) shows the same area in Fig. 6. The fence around the nickel smelter can clearly be seen and is marked in Fig. 7(a) with F1, F2, F3 and F4. In optical images such as WorldView-2 or Google Earth this fence is hardly visible. The fence is bright (grey level) in Fig. 7(a) and is partly coloured in Fig. 7(b) due to look angle differences. Both Fig. 7(a) and Fig. 7(b) show the trains going in and out from the nickel smelter, marked T1, T2 and T3 in Fig. 7(b). In Fig. 7(a) the buildings inside the fence are mostly bright which means no changes, however, there are many coloured features in Fig. 7(b) due to look angle variations. In the parking area (we checked an optical image to confirm a parking area) P5 there are few cars in Fig. 7(b), that is on 7, 8 and 9 January. From Fig. 7(a) it seems there are most cars on 8 January and 19 January. Along the roads in the lower part of the images, there seems to be no changes in Fig. 7(b). However, in Fig. 7(a) there are red stripes along the roads, which means that there is higher backscatter on 8 January than on 19 January and 10 February. We checked the snow depth on the three dates at Nyrud weather station in Norway which is 50 km from Nikel. The snow depths were 37 cm, 41 cm and 57 cm, respectively. The snow plough truck may have changed the bank of snow some places during this time.

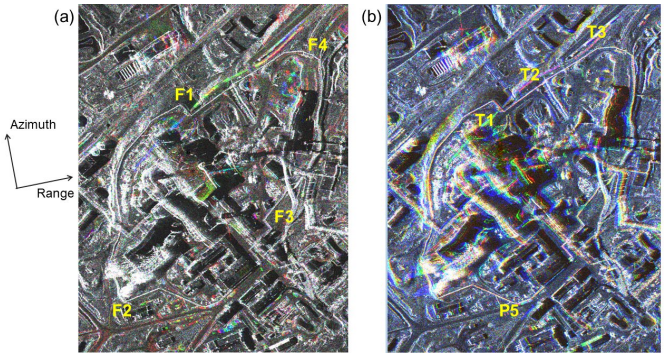

Fig. 7. (a) RGB colour composite in window W3 in Fig. 5. Azimuth and range are shown for (a). (b) RGB colour composite in the same area as in (a) in Fig. 6.

In Fig. 8 we have processed a time series of 6 geocoded coherence images at incidence angle 35.0° from the CoSSC interferometric pairs in Table II. The StInSAR DEMs were used for geocoding of the coherence images. As we see from Table II the mean coherence of the images is very high due to the subarctic winter conditions and short time (10s) between the acquisitions and is quite stable as function of time. The maximum and the minimum temperatures for the scenes processed in Fig. 8 are given in Table III. Fig. 8(e) shows a significantly lower coherence than the other scenes. If we look at Table III we see that that both the minimum and maximum temperatures this day are above zero, which means thawing. On the ice-covered power lake there are some shapes which have lowered coherence on this day.

TABLE III
MAXIMUM AND MINIMUM TEMPERATURES AT SVANVIK

Date	Max. temp. (°)	Min. temp. (°)
23 December 2014	-15.3	-26.3
3 January 2015	-1.8	-7.6
14 January 2015	-11.6	-24.1
16 February 2015	-4.9	-9.8
27 February 2015	2.3	-0.4
10 March 2015	2.0	-11.1

Svanvik is in Norway about 10 km from Nikel in Russia.

We select the left half of Figs. 8(b), (c), (d), (e) and (f) and take the difference of the images 8(c)-8(b), 8(e)-8(d), and 8(f)-8(e) and show them in Figs. 9(a), 9(b) and 9(c), respectively. In Fig. 9(a) there is not much change from most of the ground. However, the coherence in most of the river from the region near the nickel smelter down to Pasvik power lake has increased about 0.4-0.5 from 3 -14 January. From Table III we see that the minimum temperature changed from -7.6° to -24.1° and the river has probably frozen. It is however remarkable that the coherence is very low (green colour) on both 23 December and 3 January when it is quite cold. In Fig. 9(b) the coherence again drops in the river. The maximum temperature increases from -4.9° to 2.3°, which may be caused

This article has been accepted for publication in a future issue of this journal, but has not been fully edited. Content may change prior to final publication. Citation information: DOI 10.1109/JSTARS.2021.3069018, IEEE Journal of Selected Topics in Applied Earth Observations and Remote Sensing

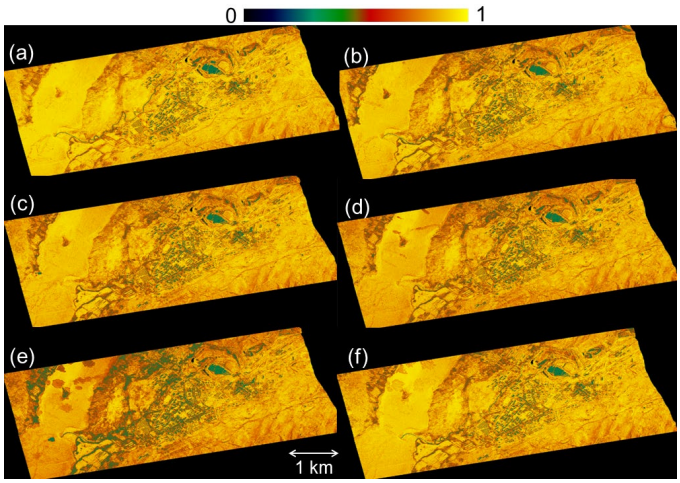

Fig. 8. Time series of UTM geocoded coherence images at incidence angle 35°. (a) 23 December 2014. (b) 3 January 2015. (c) 14 January 2015. (d) 16 February 2015. (e) 27 February 2015. (f) 10 March 2015.

by thawing in the river. We also see a dark blue shape in the ice on the Pasvik power lake which seems to be manmade where the coherence has dropped about -0.5, which means that there is probably open water. It is just outside where the river flows into the Pasvik power lake. In Fig. 8(f) this shape has disappeared and the open water is probably frozen. This can clearly be seen in Fig. 9(c) where the coherence change is about 0.5 (yellow). Further north on the lake there are some beautiful natural shapes with reduced coherence (Fig. 8(e)). Those are are probably wetter than the surroundings. In Fig. 9(c) they seem to have partly frozen again.

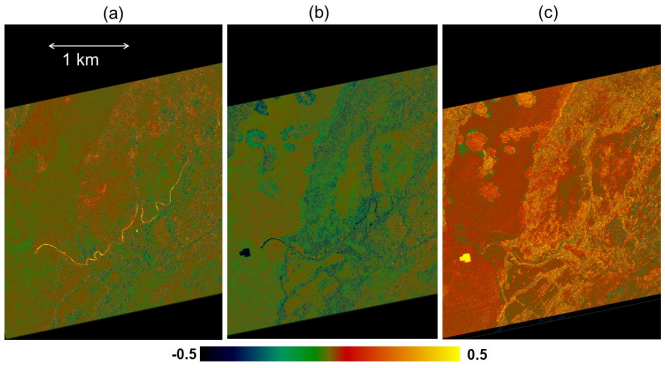

Fig. 9. Estimated coherence change selected from Fig. 8. (a) Change from 8 (b) to 8(c), change from 8(d) to 8(e), change from 8(e) to 8(f). Pixel spacing is 1.8 m.

Fig. 10(b) shows an enlarged image in the left part of Fig. 8(e) and Fig. 10(a) is the corresponding amplitude (backscatter) image. We can see that the natural shapes are also visible in the amplitude image which means that the backscatter is reduced compared to the surroundings. The supposed manmade shape is surprisingly not visible at all in the amplitude image. One possible explanation is that there is some wind on the open water in the hole in the ice. South of the river there are some green belts. These are trees between some agricultural fields which can be identified in WorldView-2 optical images or Google Earth over the same region. These trees are very difficult to detect in the amplitude image in Fig. 10(a). The forest belts are visible in all images in Fig.8, however, the strongest volume decorrelation occur in Fig. 8(e).

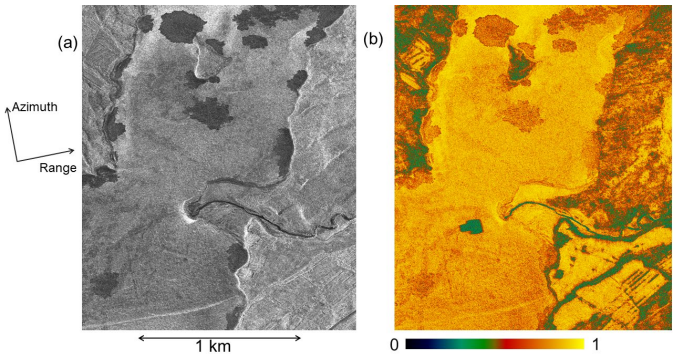

Fig. 10. (a) Amplitude image of an area in Fig. 8(e). (b) Enlarged coherence image in the lower left corner of Fig. 8(e). Pixel spacing is 1.8 m.

V. Conclusion

We have analysed coherent and incoherent changes in TDX/TSX interferometric images from the science phase. By using geocoded images we could generate RGB colour composite with only one day interval between the images. This could be very useful for future missions since change detection can be done more effectively in an interesting area by using time series of geocoded images with different look angles. Using the staring spotlight mode gives us the possibility to analyse changes in infrastructure, such as buildings and parking areas, and also natural changes. Time series of coherence images may reveal changes that are not detectable in amplitude images. An impressive precision of the overlapping area of series of both time and look angle of TSX/TDX staring spotlight images has been demonstrated in this work.

Acknowledgment

This work was supported by the Norwegian Defence Research Establishment (FFI). We very much appreciate kind help from the science team at DLR, Thomas Busche and Irena Hansjek at DLR for planning and delivery of CoSSC TanDEM-X data (AO-project NTI_INS6664). Thanks to Research Manager Richard B. Olsen at FFI and the anonymous reviewers for giving valuable comments to the manuscript.

References

[1] G. Krieger, M. Zink, M. Bachmann, M. Bräutigam, D. Schulze, M. Martone, P. Rizzoli, U. Steinbrecher, J. W. Antony, F. De Zan, I. Hajnsek, K. Papathanassiou, F. Kugler, M. R. Cassola, M. Younis, S. Baumgartner, P. López-Dekker, P. Prats, A. Moreira, "TanDEM-X: A Radar Interferometer with Two Formation Flying Satellites," *Acta Astronatica*, vol. 89, pp. 1015-1027, 2016.

[2] K. Eldhuset, "Combination of stereo SAR and InSAR for DEM generation using TanDEM-X spotlight data," *International Journal of Remote Sensing*, vol. 38, no. 15, pp. 4362–4378, May 2017.

[3] T. Kraus, B. Bräutigam, J. Mittermayer, S. Wollstadt, C. Grigorov,

"TerraSAR-X Staring Spotlight Mode Optimization and Global Performance Predictions," *IEEE Journal of Selected Topics in applied Earth Observations and Remote Sensing*, vol. 9, no. 3, pp. 83-98, 2013.

[4] I. Hajnsek, A. Moreira, M. Zink, S. Buckreuss, T. Kraus, M. Bachmann, T. Busche, "TanDEM-X: Mission status and science activities," in *Proc. International Geoscience Remote Sensing Symposium,* Yokohama, Japan, 28 July-2 Aug, 2019.

[5] A.V. Monti-Guarnieri , M.A. Brovelli, M. Manzoni, M.M. d'Alessandro, M.E. Molinari, and D. Oxili,
"Coherent Change Detection for Multipass SAR," *IEEE Trans. Geosci. Remote Sens.*, vol. 56, no. 11, pp. 6811-6822, Nov. 2018.

[6] A. Ferretti, A. Fumagalli, F. Novali, C. Prati, F. Rocca, and A. Rucci,
"Coherent Change Detection for Multipass SAR," *IEEE Trans. Geosci. Remote Sens.*, vol. 49, no. 9, pp. 3460-3470, Sep. 2011.

[7] I. Hajnsek, T. Busche, G. Krieger, M. Zink, D. Schulze and A. Moreira, 2014. "Announcement of Opportunity: TanDEM-X Science Phase." [Online] Available:https://tandemx-science.dlr.de/pdfs/TD-PD-PL_0032TanDEM-X_Science_Phase.pdf

[8] U. Balss, H. Breit, S. Duque, T. Fritz, and C. Rossi, 2012. "Payload Ground Segment: CoSSC Generation and Interferometric Considerations." [Online] Available: https://tandemx-science.dlr.de/pdfs/TD-PD-PL_0032TanDEM-X_Science_Phase.pdf

[9] K. Eldhuset and D. J.Weydahl, "Geolocation and Stereo Height Estimation Using TerraSAR-X Spotlight Image Data," *IEEE Trans. Geosci. Remote Sens.,* vol. 49, no. 10, pp. 3574-3581, Oct. 2011.

[10] K. Eldhuset and D. J.Weydahl, "Using stereo SAR and InSAR by combining the COSMOSkyMed and the TanDEM-X mission satellites for estimation of absolute height," *International Journal of Remote Sensing,* vol. 34, no. 23 , pp. 8463-8474, 2013.

[11] R. L. Lillestøl, K. Eldhuset, T. N. Hannevik, A. O. Knapskog, R.B. Olsen and K. O. Viken, "Anvendelser av SAR-bilder fra satellitter over land," Norwegian Defence Research Establishment, Kjeller, Norway, Tech. Rep. 19/01695,2019.[Online].Available:https://www.ffi.no/publikasjoner/arkiv/anvendelser-av-sar-bilder-fra-satellitter-over-land

[12] Y. Sun, L. Lei, D. Guan, S. Wollstadt, X. Li, and G. Kuang,
"SAR Image Change Detection Based on Nonlocal Low-Rank Model and Two-Level Clustering," *IEEE Journal of Selected Topics in applied Earth Observations and Remote Sensing*, early access.

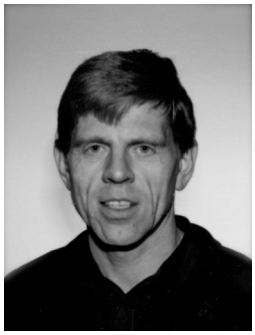

Knut Eldhuset was born in 1958 and received the cand. scient. degree (M.Sc.) in nuclear physics in 1983 from the University of Oslo and the dr. scient. degree (Ph.D.) in physics/signal processing (1987) from the University of Tromsø. He has been with the Norwegian Defence Research Establishment (FFI) since 1983, working on processing and applications of satellite Synthetic Aperture Radar (SAR) data. His research interests cover a wide range of topics, including orbit simulation, geolocation, automatic ship detection, SAR/scanSAR processing, InSAR processing, scattering theory, polarimetry, MTI simulations and processing of bi-static SAR data. His results have contributed to numerous national projects, to European defence research projects and to several studies for the European Space Agency. He has developed advanced algorithms for ship and wake detection, and for SAR processing using the Extended Exact Transfer Function (EETF), both of which were developed into commercial products by the Kongsberg Group. The latest SAR processing algorithm is the Decomposed Transfer Function (DTF). While his early work was focused on ERS, ENVISAT and Radarsat-1, his more recent work has focused on polarimetric analysis of Radarsat-2 images and InSAR combined with stereoSAR using TerraSAR-X/TanDEM-X and COSMO-SkyMed for DEM generation.